


RESEARCH ARTICLE | MARCH 14 2024

Centralized design and production of the ultra-high vacuum and laser-stabilization systems for the AION ultra-cold strontium laboratories ^{EP}

Special Collection: [Large Scale Quantum Detectors](#)

B. Stray; O. Ennis; S. Hedges; S. Dey; M. Langlois; K. Bongs; S. Lellouch; M. Holynski; B. Bostwick; J. Chen; Z. Eyler; V. Gibson; T. L. Harte; C. C. Hsu; M. Karzazi; J. Mitchell; N. Mouelle; U. Schneider; Y. Tang; K. Tkalcec; Y. Zhi; K. Clarke; A. Vick; K. Bridges; J. Coleman; G. Elertas; L. Hawkins; S. Hindley; K. Hussain; C. Metelko; H. Throssell; C. F. A. Baynham; O. Buchmüller ; D. Evans; R. Hobson; L. Iannizzotto-Venezze; A. Josset; E. Pasatembou; B. E. Sauer; M. R. Tarbutt; L. Badurina; A. Beniwal; D. Blas; J. Carlton; J. Ellis; C. McCabe; E. Bentine; M. Booth; D. Bortoletto; C. Foot; C. M. Gómez-Monedero Castellanos; T. Hird; K. Hughes; A. James; A. Lowe; J. March-Russell; J. Schelfhout; I. Shipsey; D. Weatherill; D. Wood; S. Balashov; M. G. Bason; J. Boehm; M. Courthold; M. van der Grinten; P. Majewski; A. L. Marchant; D. Newbold; Z. Pan; Z. Tam; T. Valenzuela; I. Wilmot



AVS Quantum Sci. 6, 014409 (2023)

<https://doi.org/10.1116/5.0172731>

Centralized design and production of the ultra-high vacuum and laser-stabilization systems for the AION ultra-cold strontium laboratories

Cite as: AVS Quantum Sci. 6, 014409 (2024); doi: 10.1116/5.0172731

Submitted: 18 August 2023 · Accepted: 6 February 2024 ·

Published Online: 14 March 2024




View Online



Export Citation



CrossMark

B. Stray,¹ O. Ennis,¹ S. Hedges,¹ S. Dey,¹ M. Langlois,¹ K. Bongs,¹ S. Lellouch,¹ M. Holynski,¹ B. Bostwick,² J. Chen,² Z. Eyler,² V. Gibson,² T. L. Harte,² C. C. Hsu,² M. Karzazi,² J. Mitchell,² N. Mouelle,² U. Schneider,² Y. Tang,² K. Tkalcec,² Y. Zhi,² K. Clarke,³ A. Vick,³ K. Bridges,⁴ J. Coleman,⁴ G. Elertas,⁴ L. Hawkins,⁴ S. Hindley,⁴ K. Hussain,⁴ C. Metelko,⁴ H. Throssell,⁴ C. F. A. Baynham,⁵ O. Buchmüller,⁵  D. Evans,⁵ R. Hobson,⁵ L. Iannizzotto-Venezze,⁵ A. Josset,⁵ E. Pasatembou,⁵ B. E. Sauer,⁵ M. R. Tarbutt,⁵ L. Badurina,⁶ A. Beniwal,⁶ D. Blas,^{6,a)} J. Carlton,⁶ J. Ellis,⁶ C. McCabe,⁶ E. Bentine,⁷ M. Booth,⁷ D. Bortoletto,⁷ C. Foot,⁷ C. M. Gómez-Monedero Castellanos,⁷ T. Hird,⁷ K. Hughes,⁷ A. James,⁷ A. Lowe,⁷ J. March-Russell,⁷ J. Schelfhout,⁷ I. Shipsey,⁷ D. Weatherill,⁷ D. Wood,⁷ S. Balashov,⁸ M. G. Bason,⁸ J. Boehm,⁸ M. Courthold,⁸ M. van der Grinten,⁸ P. Majewski,⁸ A. L. Marchant,⁸ D. Newbold,⁸ Z. Pan,⁸ Z. Tam,⁸ T. Valenzuela,⁸ and I. Wilmut⁸ (AION collaboration)

AFFILIATIONS

¹Physics and Astronomy, University of Birmingham, Edgbaston, Birmingham B15 2TT, United Kingdom

²Cavendish Laboratory, University of Cambridge, J J Thomson Avenue, Cambridge CB3 0HE, United Kingdom

³ASTeC, STFC Daresbury Laboratory, Warrington WA4 4AD, United Kingdom

⁴Department of Physics, University of Liverpool, Merseyside L69 7ZE, United Kingdom

⁵Department of Physics, Blackett Laboratory, Imperial College, Prince Consort Road, London SW7 2AZ, United Kingdom

⁶Physics Department, King's College London, Strand, London WC2R 2LS, United Kingdom

⁷Department of Physics, University of Oxford, Parks Road, Oxford, OX1 3PU, United Kingdom

⁸STFC Rutherford Appleton Laboratory, Didcot OX11 0QX, United Kingdom

Note: This paper is part of the Large Scale Quantum Detectors Special Issue.

a) Present address: Grup de Física Teòrica, Departament de Física, Universitat Autònoma de Barcelona, 08193 Bellaterra, Barcelona, Spain and Institut de Física d'Altes Energies (IFAE), The Barcelona Institute of Science and Technology, Campus UAB, 08193 Bellaterra, Barcelona, Spain.

ABSTRACT

This paper outlines the centralized design and production of the ultra-high-vacuum sidearm and laser-stabilization systems for the AION Ultra-Cold Strontium Laboratories. Commissioning data on the residual gas and steady-state pressures in the sidearm chambers, on magnetic field quality, on laser stabilization, and on the loading rate for the 3D magneto-optical trap are presented. Streamlining the design and production of the sidearm and laser stabilization systems enabled the AION Collaboration to build and equip in parallel five state-of-the-art Ultra-Cold Strontium Laboratories within 24 months by leveraging key expertise in the collaboration. This approach could serve as a model for the development and construction of other cold atom experiments, such as atomic clock experiments and neutral atom quantum computing systems, by establishing dedicated design and production units at national laboratories.

© 2024 Author(s). All article content, except where otherwise noted, is licensed under a Creative Commons Attribution (CC BY) license (<http://creativecommons.org/licenses/by/4.0/>). <https://doi.org/10.1116/5.0172731>

I. INTRODUCTION

The Atom Interferometer Observatory and Network (AION) project^{1,2} is developing quantum technologies using cold atoms for a novel class of fundamental physics experiments. These will enable

searches for ultralight dark matter and measurements of gravitational waves from astrophysical and cosmological sources in the deci-Hz frequency band that is inaccessible to other current and planned experiments.³ These sources may include black holes with masses

intermediate between those discovered by the LIGO and Virgo experiments and the heavier black holes known to be present in galactic nuclei.⁴

AION will demonstrate the required deployable and scalable quantum technology by constructing and operating staged 10 and 100 m-scale instruments, paving the way for a future kilometer-scale facility and a possible spaceborne atom interferometer experiment, such as AEDGE.⁵ In the first phase of stage 1 of the AION project, funded via the UKRI QTFP program,⁶ a joint STFC and EPSRC team has successfully delivered a new collaborative network in cold-atom interferometry, and by spring 2024, this collaboration will have made key steps toward the construction and deployment of a first 10-m prototype instrument.

The AION project requires the state of the art in single-photon strontium atom interferometry to be developed to new levels. To this end, one of the main deliverables of the AION project in its first phase of funding was to build dedicated Ultra-Cold Strontium Laboratories (UCSLs) tasked with conducting complementary R&D efforts in parallel, at the University of Birmingham (Large Momentum Transfer), the University of Cambridge (transport, cooling, launch and atom optics), Imperial College London and the Rutherford-Appleton Laboratory (RAL) (squeezing and high-intensity atom interferometry), and the University of Oxford (atom sources and location of the AION-10 detector).

Coordinating the parallel delivery of five state-of-the-art UCSLs within 24 months represented a new challenge for cold atom physics, and is a keystone of any future cold-atom infrastructure project. In order to accomplish this ambitious goal, the AION project adopted an approach that is well established in, e.g., the particle physics community, of centralizing the design and production of key components of the UCSLs, namely, the ultra-high vacuum (UHV) and laser-stabilization (LS) systems.

Traditionally, such systems are designed and built in-house by each laboratory, requiring significant staff and time resources in each location. By leveraging key expertise within institutions in the collaboration, such as in LS at Imperial College London, in oven and source design at the University of Oxford, in static and tunable-focus dipole traps at the University of Cambridge, and the expertise in UHV

construction at the RAL and Daresbury national laboratories, it was possible to streamline the design and production of both UHV and LS systems. This required establishing a high level of collaboration across all UCSLs, which greatly shortened the resource required at each individual institution to build the five UCSLs compared to the traditional approach.

This document summarizes the approach and methods utilized for the centralized design and production of the UHV and LS systems for the AION UCSLs, which could serve as a useful model for the modular and distributed development and construction of other cold atom experiments, such as atomic clock experiments or neutral atom quantum computing systems. Commissioning data on the performances of the UHV and LS systems are also presented. The AION project is currently investigating the possibility of commercializing the centralized design and production of the UHV and LS systems, facilitating broader use of this approach for other cold atom projects. It should be noted that the optical designs and control systems were also centralized but are not discussed in this document.

II. LASER COOLING OF STRONTIUM—REQUIREMENTS

In the planned atom interferometers, the atoms will be cooled and prepared in dedicated UHV chambers mounted to the side of the vertical main interferometer tube before being transported into the main tube for launching and atom interferometry.¹ These auxiliary chambers are referred to as *sidearms* and their specifications regarding structure, magnet systems, and parts of the laser stabilization system are driven by the laser cooling techniques used to generate cold strontium clouds. The laser cooling scheme employed by AION is depicted in Fig. 1.

The AION cooling sequence follows a similar pattern as previous experiments with cold strontium:^{7,8}

1. Effusion of atoms from a hot strontium oven;
2. Capture of atoms in a 2D “blue” magneto-optical trap (MOT) in chamber 1, creating a beam of slow atoms;
3. Recapture of the slow beam in a 3D blue MOT in chamber 2;
4. Further cooling to 1 μ K in a 3D “red” MOT;
5. Loading into an optical dipole trap for evaporative cooling;

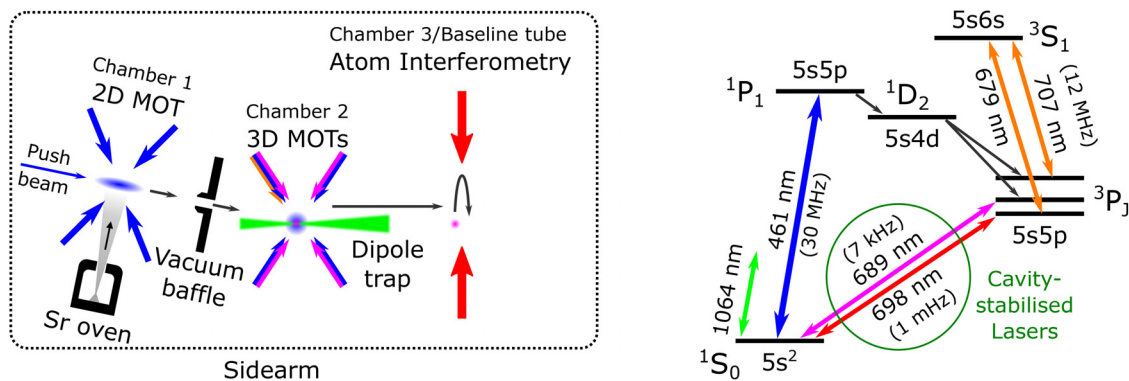


Fig. 1. Left: Conceptual schematic of an AION sidearm, depicting the strontium laser cooling regions. The magneto-optical traps (MOTs) are created inside ultra-high vacuum chambers (see Sec. III A) and require several laser beams (see Sec. IV) as well as externally applied magnetic fields (see Sec. III B). Right: Strontium level scheme, showing the laser wavelengths used for cooling, trapping, and interferometry. Linewidths are given in brackets. The $5S5p\ ^3P_0$ state has 1 mHz linewidth for the ^{87}Sr isotope used in AION; in the even isotopes $^{88,86,84}\text{Sr}$, the state is much narrower because single-photon decay is strictly forbidden. The 3P_J levels are ordered $J = 0, 1, 2$ from bottom to top.

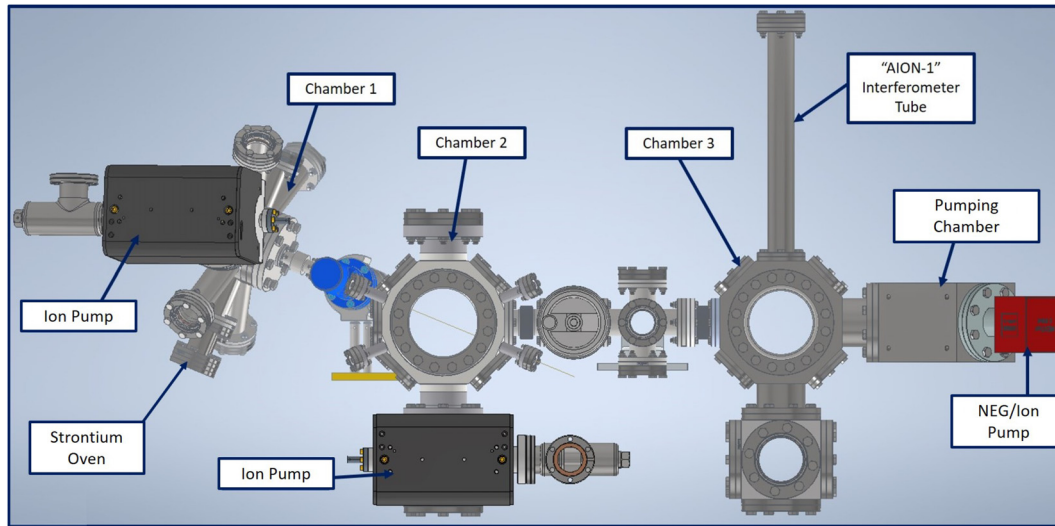


FIG. 2. The layout of the three-chamber vacuum systems at the Universities of Cambridge and Oxford.

6. Optical transport into the atom interferometry region (either chamber 3 in test sidearms or the main vertical tube in the full-scale detector);
7. Atom launch, interferometry, and measurement.

The layout of the three-chamber vacuum systems at the Universities of Cambridge and Oxford is shown in Fig. 2.

All stages in the cooling sequence must be carried out in an ultra-high vacuum environment, to reduce background gas collisions to a negligible rate. Pressures of $\leq 10^{-10}$ mbar are required in chambers 2 and 3 to ensure negligible background atom loss during evaporative cooling in chamber 2 and atom interferometry in chamber 3. The AION vacuum system meeting these requirements is described in Sec. III A.

For stages 1–3 of the sequence, strong magnetic field gradients in chambers 1 and 2 are required. In chamber 1, these fields can be applied permanently through the use of NdFeB permanent magnets that reduce power consumption and cooling requirements. In the case of chamber 2, high-current water-cooled coils are needed to make the required magnetic field gradient—see Sec. III B.

The stages of the sequence addressing narrow transitions (red MOT; atom interferometry) require narrow-linewidth, cavity-stabilized lasers at 689 and 698 nm, whereas the stages that address broader transitions (blue MOT; repumping transitions) or use far off-resonance light (dipole trap) rely on wavemeter-locked lasers at 461, 679, 707 nm, and free-running lasers at 1064 nm—see Sec. IV.

III. SIDEARM SYSTEM

A. Ultra-high vacuum system

1. Overview

Although the overall designs of the five vacuum systems are similar, their precise designs vary slightly according to the intended R&D work to be undertaken with each sidearm. Unless otherwise mentioned, this document describes the full three-chamber sidearm used at

the Universities of Oxford and Cambridge. The sidearms used at Imperial College, RAL and the University of Birmingham do not include chamber 3, and the Birmingham sidearm includes an extra six-way cross and tube on chamber 2 to facilitate development of large momentum transfer atom interferometry sequences.

Chamber 1, shown in Fig. 2, contains the strontium oven, which is illustrated in Fig. 3, whose presence limits its attainable vacuum pressure. For this reason, chambers 1 and 2 have separate ion pumps with the transfer line between the two containing a differential pumping aperture of 3 mm diameter and 15 mm length. Chamber 1 has multiple viewports, four of which are in the required configuration for the 2D MOT. These are outside the line-of-sight of the oven, so as to ensure that they are not coated with strontium when the oven is operating. The background vacuum level in chamber 1 was required to be lower than 10^{-9} mbar in order not to affect the base pressure in the adjoining chamber. The chamber is processed, built, and tested to the same standards as the rest of the vacuum system.

Chamber 2 includes the 3D MOT chamber and the one or two cubes that sit below, depending on the system specification. All of chamber 2 is pumped by a single 20 l/s ion pump and a NEG cartridge pump that connects to the cube directly beneath the chamber. Chamber 3 is located beyond chamber 2, connected through a gate valve, and the transition from chamber 2 to chamber 3 represents the transition from the sidearm to the interferometer tube. Chamber 3 (present only in the Oxford and Cambridge assemblies) has no magnets and only optical access. Chamber 3 is used, along with its associated extension tube, as a proxy for a 1 m interferometer. The launch optics are housed around the 6-way cube below the chamber. Chamber 3 is pumped from a final “pump chamber” with a NEG-ion pump.

2. Design

The design of the vacuum system and associated support frame was driven by a variety of requirements. These included the common

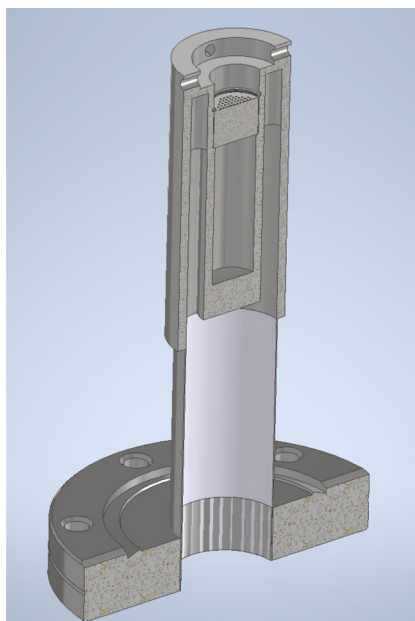


FIG. 3. The stainless steel oven for heating strontium. The six cartridge heaters and two thermocouples (not shown) are inserted from the rear (bottom of drawing) without the need for any electrical feedthroughs. A thin-walled stainless steel tube of low thermal conductance connects the cylindrical oven body to a Conflat flange (CF40). The nozzle was laser machined from a stainless steel disk and held in place by a C-clip (150 circular channels of 0.3 mm diameter and 3 mm long) and mounted within a recess in the oven body to reduce thermal losses (cf. mounting flush with the end of the cylinder).

requirements of such a system, such as vacuum performance, ability for bake-out, access to the magnet system, optical access, and operational stability. In addition, the centralized production drove additional requirements, namely, strength and stability for transport, installation and servicing access, and methodology at the destination institutions and the ability to manufacture efficiently or procure vacuum components. The solutions to the above-mentioned requirements benefited from a centralized engineering approach in a number of ways.

A key metric for the vacuum systems is their vacuum quality, as collisions with background gas atoms ultimately limit the lifetime of ultra-cold atoms and can thereby limit the duration of the experimental sequence. Furthermore, it was critical that this performance be consistent across all five systems, as inconsistent vacuum levels between the five systems could lead to difficulties when transitioning technology between the sidearms. The ability to transfer technology seamlessly between institutions is a major requirement of the systems, as key deliverables rely on the integration of the technologies developed in the five UCSLs into a single system to demonstrate interferometry on the clock transition. Centralizing the design of the system and specification of the pumping strategy ensured that the project optimized the prospects for achieving the required similarity of performance between systems.

Ancillary system integration had to be considered at a fundamental and conceptual design level because these systems interface very closely with the vacuum system. A poorly considered fastener arrangement or an unstable mount could ultimately cause a catastrophic leak

in the system. This was especially relevant for the permanent magnets and electromagnetic coils required for the MOTs in chambers 1 and 2 (see Sec. III B for more detailed information on these systems). These magnet systems are installed after the vacuum system has been sealed, evacuated, baked out, and signed off, and any failure of the vacuum system during installation might require transport back to the build facility, partial-rebuild, and re-bake. A particularly striking example of this is the installation of the electromagnetic coils for chamber 2 MOT (the 3D MOT). Installation of one half of these coils presented a potential issue in the form of a clash between the coils and the gate valve separating chambers 1 and 2. A common modular mounting system was, therefore, designed for all sidearms, which would allow safe installation of the coils retrospectively onto the vacuum system.

Subsystems and components that require methodical or detailed installation methods and techniques benefit greatly from the centralized approach as individual laboratories avoid operating at an elevated risk during the installation process. Standardization of viewport specification was an important example of this. An effort was made to ensure that, where possible, all systems had the same specifications for viewports in the same position. This allowed for central procurement and a centralized inventory of viewports that led to a decreased level of risk during the integration phase of the project, which would not have been possible had each laboratory been specifying independently the viewports required for their deliverables. The centralized inventory became invaluable during the build process when the fragility and attrition rate of the viewports became apparent during the first bakes: A substantial risk to the fragile viewports was the bakeout temperature profile, and the centralized, sequential builds enabled us to improve progressively the bakeout profile for later bakes, thereby substantially reducing the risk associated with the bake-out cycle. See Sec. III A 4 for more information on the centralized build and its benefits.

During design of the vacuum chambers for the system—see Fig. 4 for images of these chambers—the mechanical engineering team at the University of Oxford looked into the effects of material selection on magnetic permeability. Traditionally, 316LN (re-annealed after machining or fabrication) has always been specified for vacuum systems where low magnetic permeability has been required. The Oxford team looked into the effects of the inherent stresses of traditional machining (milling, turning, honing, grinding, etc.) on the material and how re-annealing the material relaxes and dissipates these stresses. It was observed that reducing the stresses experienced by the material during the manufacturing process resulted in a reduced magnetic permeability of the final part. In the end, the mechanical engineering team was able to use electrical discharge machining (EDM), a force-free machining process, to create low magnetic permeability vacuum components out of 316L at a reduced cost. Wire cutting was used for the majority of the machining, using spark erosion with a custom electrode in some places, to form non wire-cut features. The centralized approach facilitated this quasi-independent research and the bulk manufacture of components for vacuum systems. Each system benefited performance-wise and economically from this work, making this endeavor cost-neutral.

3. Designing the sidearm packaging

From the onset of the project, the sidearms were conceived as development platforms toward the AION-10 and AION-100 projects. A sidearm for an AION-10 or AION-100 application would require

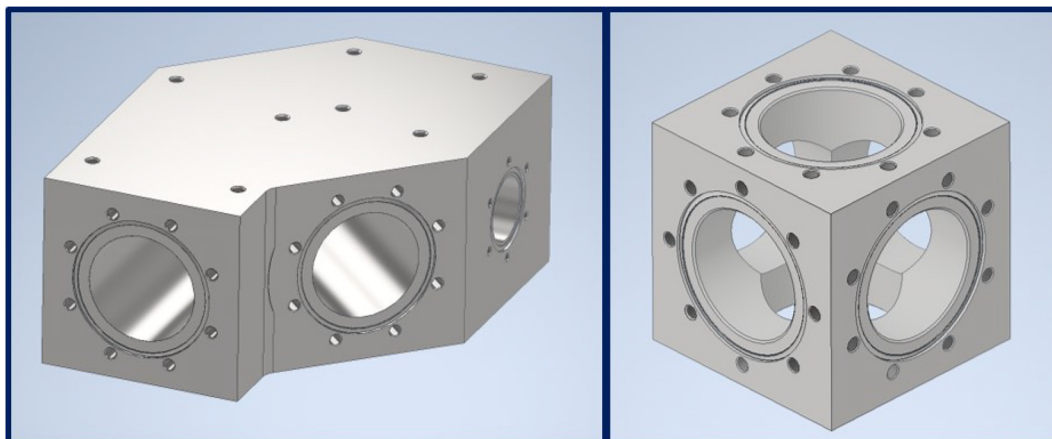


Fig. 4. (Left) The NEG pump chamber and (right) the interferometer cube, which were fabricated from 316L using EDM as described in the text.

packaging. The choice to package the sidearm into a single transportable object that could be delivered to each institution (or by extension an AION-10 or AION-100 construction site) was one of the key decisions that enabled the manufacture to be centralized.

The constraints on the packaging of the sidearm were minimal. It needed to be self-contained, transportable, robust, and large enough to accommodate most or all of the optical systems that would need to be integrated around it.

The initial sidearm packaging concept included an optical table as the base on which the vacuum system and other components would be assembled. In order to increase their flexibility as a development platform and to stay closer to the eventual requirements of AION-100, a choice was taken to simplify this and instead to mount the packaged sidearm on existing optical tables. With hindsight this choice complicated matters considerably, as there needed to be many removable parts, and a complex transfer process to fit the sidearm onto existing optical tables.

There were five sidearms built in a total of four varieties so as to enable the exploration of different areas of the sidearm development in different institutes, as discussed above. The design started with the package for the Universities of Oxford and Cambridge, which was the most complex, and packaged it in such a way that it could be shortened for RAL and Imperial College, and could in turn be made taller for the University of Birmingham. The four versions of the packaging frame are all based on a common design and the variations are well understood, enabling further developments of laser systems and system operation. Although the customization of the basic design for different institutions increased the complexity and engineering cost, it enabled them to follow different R&D paths while still benefiting significantly from the common framework.

One area that was not considered sufficiently at the design phase was defining a suitable dimensioning scheme to mount the vacuum system in the packaging frames. The packaging frame was essentially a cuboid and provided a reasonable set of datums. However, the location of the parts of the vacuum system was not defined with respect to this frame, and it was not checked that the assembly tolerances were compatible. The lack of consistent dimensioning led to the vacuum chambers having to be tweaked into place when the whole system was

almost complete, and success was not guaranteed until the final adjustments were made. In future, such a system should recognize that, whereas there need not be any requirement on how the vacuum system sat in the frame, there is a need to specify positions to facilitate accurate assembly.

4. Processing and assembly of the vacuum systems

The AION sidearms have a modular design similar to accelerators and hence lend themselves to Daresbury Laboratory Engineering Technology Center facility's construction processes. As an STFC National Laboratory facility, this Center is set up to deliver "plug and play" modules to major national and international accelerator projects. Although the instrument is predominately a vacuum system, the AION project called on the Center's in-house mechanical workshop for modifications to components and the electrical technicians to provide power to the ion pumps during transportation and control of the strontium oven. Rigging effort was also used to move systems and crates for delivery. Having these teams under one roof kept the build progressing in a timely and efficient manner.

The bulk of the AION build was conducted through the Center's vacuum processing laboratory, where high-precision cleaning and temperature processes are used to reach UHV specifications, such as those required by the AION project and many accelerators. The facility utilizes a scientifically designed cleaning process to prepare vacuum components to achieve specified vacuum levels. The process uses a high-pressure detergent rinse and ultrasonic solvent cleaning to remove any hydrocarbons from the surface. Some components were then vacuum fired to drive hydrogen out of the stainless steel to reduce outgassing in order to improve the results of the final system bakeout. The capacity of the facility made it possible to process the components of several systems in a minimal number of batches before assembly. As the laboratory routinely handles vacuum systems, it had a stock of suitable adaptors, spares, and consumables that allowed the work to progress without unnecessary delays.

The subsystems were assembled and helium leak-checked to resolve any leaks before initial residual gas analysis (RGA) and temperature bakes of components. This highlighted a significant weakness in

TABLE I. Steady-state pressures of each of the chambers that form the sidearm after baking and several days of operation, listed by institution. Pressures are judged by the currents in the ion pumps linked to the chambers. In view of the conductance of the pump linkages, the pressures experienced by the atoms may be slightly higher. Note that the pressure in the University of Oxford chambers 2 and 3 is higher than specification due to the replacement of a failed window and no recovery bake (see the text for more details).

Institution	Pressure (mbar)		
	Chamber 1	Chamber 2	Chamber 3
Birmingham	5.7×10^{-10}	1.8×10^{-11}	...
Cambridge	4.7×10^{-10}	2.0×10^{-11}	2.1×10^{-11}
Imperial	3.4×10^{-10}	1.3×10^{-11}	...
Oxford	2.3×10^{-10}	1.6×10^{-10}	2.1×10^{-10}
RAL	2.1×10^{-10}	1.3×10^{-11}	...

the supplied commercial viewport windows and several initially failed the leak rate required for the UHV systems and others were not robust enough for a heat cycle. One of the specified coatings did not adhere well to the viewports and several seemed to deteriorate with heat cycling. The project decided to reduce their number and shuffle viewports from other systems, something which was made possible by the centralized assembly.

The heat cycle chosen for the bakeout was aimed to reduce any thermal differences across viewports and remain below the maximum allowable for the viewports, using a 5 °C per hour ramp rate and maximum of 140 °C. This maximum was reduced to 115 °C when the only available replacement windows were bonded rather than brazed. A failure of a bonded Oxford chamber 3 window on the final bake meant this had to be swapped to a blank flange without a bake, hence the tabulated pressure is above specification for this chamber (see Table I). Due to the project timeline, the decision was taken to ship to Oxford without an additional recovery bake: this will be completed onsite once

a replacement viewport is sourced. Optical viewports proved to be a major challenge during the assembly and commissioning and having an inventory across several systems meant replacements could be made quickly. Future projects should carry a number of spares.

Once the subassemblies had been proven to be clean and leak-tight to the appropriate level, the whole system was assembled into the frame and loaded into a large air oven for full bakeout procedure and NEG activation. Knowing that the components are clean and leak-tight before assembly into the frame reduced the risk of a major strip down to resolve problems. The system was connected to the oven turbomolecular pump, an RGA, leak detection, and bakeout were performed. Part-way through the bake, the NEG pumps were activated to allow the gas released to be pumped away to reduce chamber contamination. The ion pumps were flashed during system cool down. Once complete, the system was leak checked, another RGA scan was taken and any issues resolved. Comparing the pressures found in RGA scans before and after baking, shown in the left and right panels of Fig. 5, very substantial reductions in the residual gas pressures over a wide range of atomic mass units (AMU) can be seen. Furthermore, the centralized production approach led to an improved knowledge of expected contaminants before and after bake, and an understanding of which of these contaminants would cause vacuum issues. The scans in Fig. 5 show no presence of hydrocarbons prior to bake, and the dominant pre-bake water contaminant (AMU 18) was greatly reduced by the bakeout.

The final step was to load the strontium oven in an inert atmosphere followed by loading into the vacuum system under nitrogen purge. The vent and pump down at this point were kept to a minimum time to reduce ingress of water into the system and recover a good vacuum level. The system was then taken through a final bake cycle where the strontium oven was outgassed and run up to temperature. After final checks were complete, the system was sealed and removed from the bake oven on the transport trolley ready for packing into the crate for transport to the institutes. The vacuum pressures achieved in each of the sidearm chambers are shown in Table I.

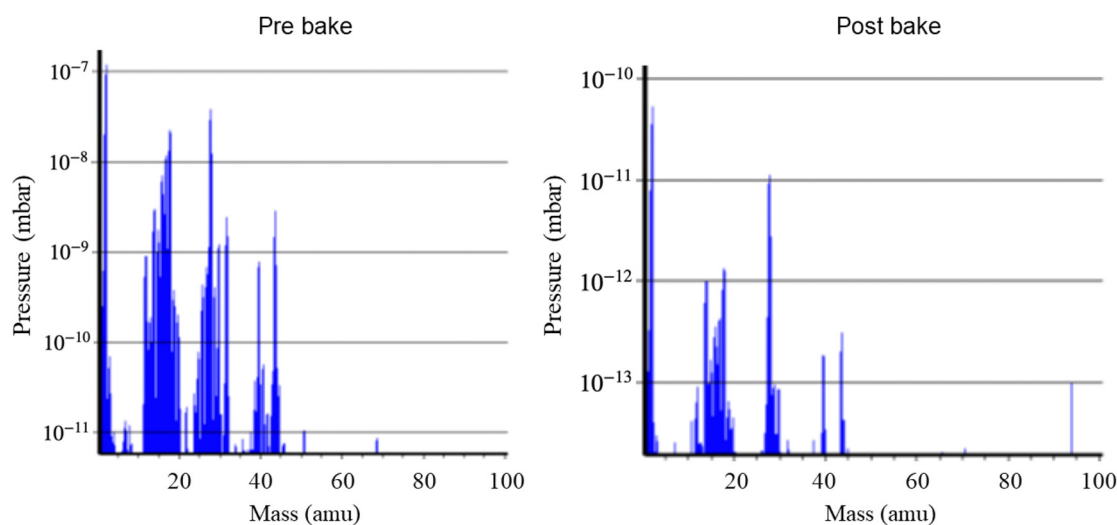


Fig. 5. RGA scans (left) pre- and (right) post-bake, indicating the cleaning of the system: note the difference between the pressure scales. Data were measured by the Daresbury Laboratory team.

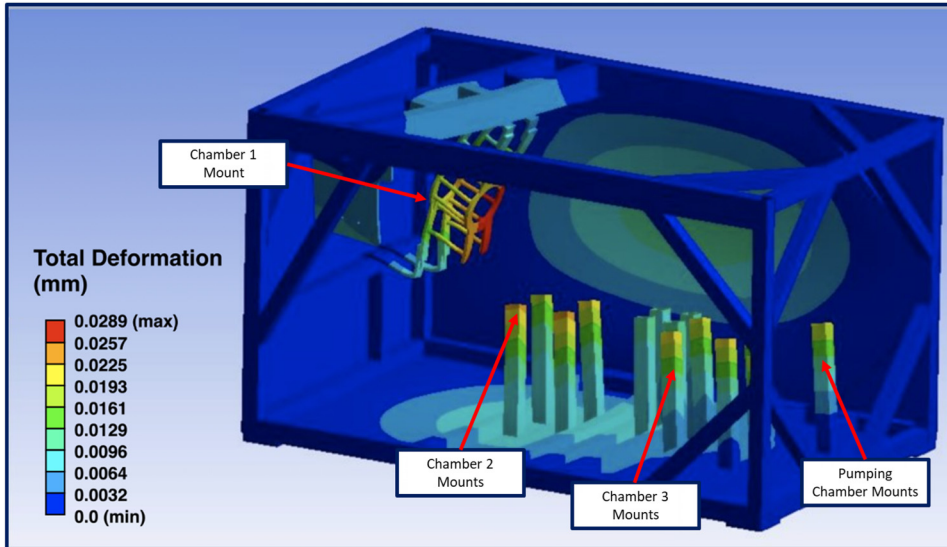


FIG. 6. Results for total displacements found in a finite element analysis (FEA) of the transport package structure, illustrating the combined use of space frame and shear plates to support the vacuum systems during transport. The vacuum chambers are hidden, but mount deflection is shown, which can be used to assess potential loading the vacuum system is subject to during transport and handling.

The fact that the facility had responsibility for several builds permitted a certain amount of parallelization. This became beneficial when a design problem was met that had to be resolved, as work could continue on subsequent builds. As the basic design was common the resolution was applied uniformly across all systems. The learning gained from the first system allowed the following ones to progress at a much faster rate. Several challenges related to the assembly from the design could be improved in subsequent iterations of the system.

5. Logistics and installation planning

The design of the transport process included vibration simulations on the sidearm with representative transport vibration spectra to ensure that no part of the system would be displaced by a problematic amount. Finite element method (FEM) studies were used for this purpose and showed the diagonal stiffness of the frame to be marginal in some cases. Therefore, the assembled vacuum system in the sidearm framework was wrapped in shear plates (6 mm thick aluminum sheet metal to provide at minimal cost substantial diagonalisation of the frame’s cuboid faces) to improve the framework’s marginally adequate racking stiffness. Figure 6 shows results from the displacement study that motivated this choice. The enclosed sidearm was then packed in a custom wooden crate along with the trolley it was built upon and a power system to keep the ion pumps running throughout the transport (see Fig. 7).

Getting the sidearm off the transport trolley could not be done by lifting as none of the destination laboratories had either built-in lifting equipment or the ability to bring in a temporary system. Instead a system of rails was designed that could be used to bridge between the transport trolley and the designated optical table (Fig. 8), and the sidearm had castors attached that were used to jack the sidearm up and roll it into position. In some instances, multiple moves were required to position the sidearm correctly in the laboratory.

Once the sidearm was placed, it was bolted down to the table and the rest of the transport framework could be dismantled from around the vacuum system. Figure 9 shows the five sidearms installed at their respective institutes. All sidearms were delivered and installed successfully without the move creating any vacuum failures. Although this

transport and delivery process was well designed, a simple change during manufacture switched away from the original brackets to through-bolted connections, which made the removal of components very complex.



FIG. 7. The University of Cambridge sidearm being unloaded with shearplates in place—showing the transport and assembly trolley and the base of the wooden shipping case.

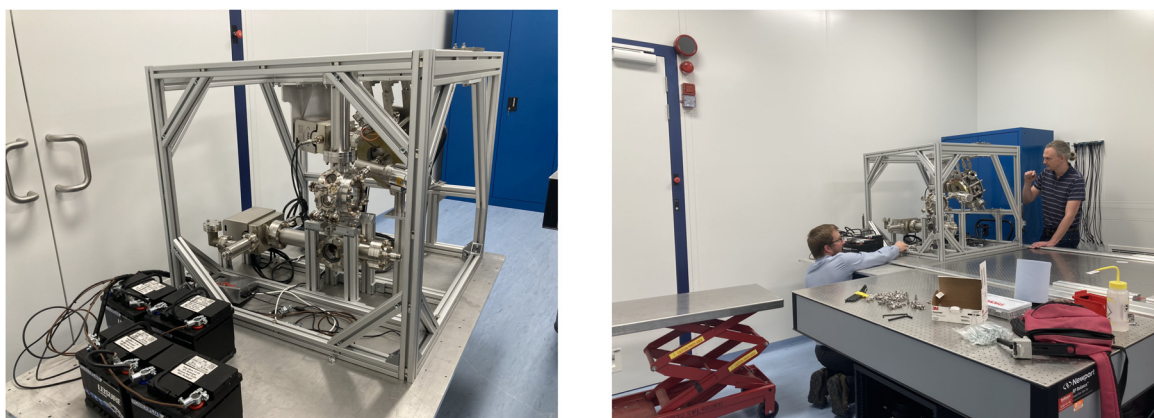


FIG. 8. (Left) The RAL sidearm on its transport baseplate following the removal of the surrounding shearplates. The batteries used to power the vacuum pumps during transport can be seen on the left of the image. (Right) Movement of the RAL sidearm from the transport trolley to the optical table using translating rails (see the text).

B. Magnet system

1. Magnetic field requirements

As described in Sec. II, the AION sidearm requires control of magnetic fields and field gradients in two locations, chambers 1 and 2, in order to facilitate the 2D MOT in chamber 1 and the blue and red 3D MOTs in chamber 2. In particular, they require a 2D quadrupole field in chamber 1 and a 3D quadrupole in chamber 2. In order to estimate the required gradients, the *AtomECS Rust* package⁹ was used to simulate the laser cooling dynamics with the goal of optimizing atom capture rates in the 3D blue MOT in chamber 2. The *MagPyLib*

Python library¹⁰ was used to determine how the required field strength could be obtained in chamber 1, and Chamber 2 magnets were simulated in *Mathematica* using the *Radia* package.

2. Magnet design—Chamber 1

Chamber 1 includes three separate magnet systems (see Fig. 10). Strong radial field gradients are provided by four assemblies of pairs of N52 NdFeB permanent magnets. Using a simplified model of the system, the simulated magnetic fields of these eight permanent magnets were shown to create a quadrupole magnetic field in its center, and the

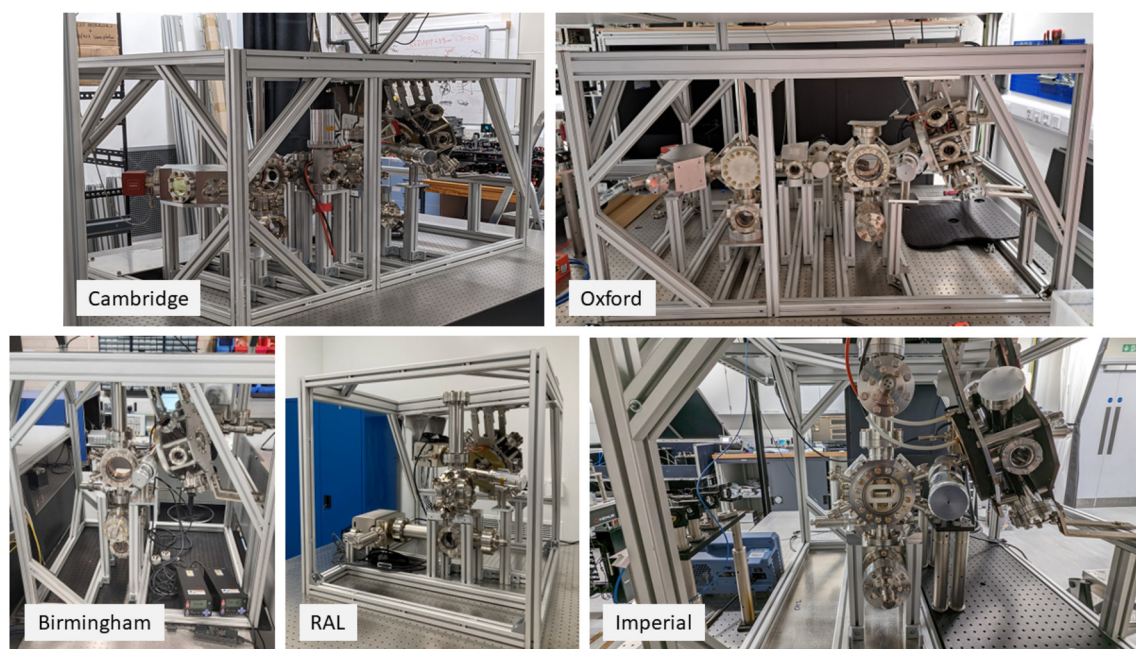


FIG. 9. The five sidearm systems, installed at their corresponding institutions.

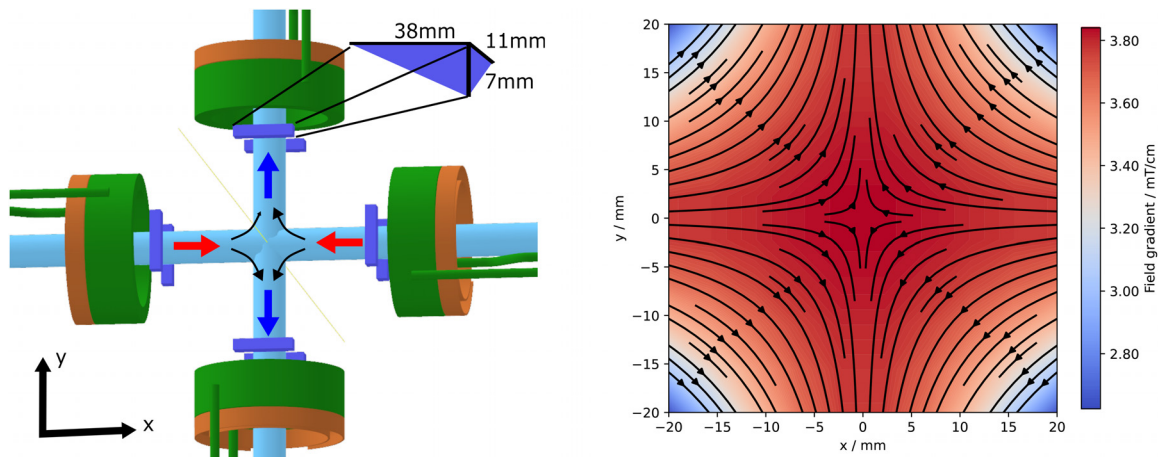


Fig. 10. (Left) Chamber 1 coil assemblies, showing permanent magnets in dark blue, trim coils in green, and heat exchangers in orange. Red (blue) arrows indicate the north (south) poles of the magnets. Doppler-cooling laser beams (light blue) counter-propagate along the x and y axes. Atoms experience cooling and confinement in the xy plane and are pushed in the z direction by an additional beam into the second chamber. (Right) Simulated magnetic field lines and gradients generated in chamber 1 at the calculated optimum parameters for atom loading in chamber 2.

AtomECS Rust package⁹ was used to optimize the atomic flux by varying the dimensions and distance of Chamber 1 permanent magnets.

The optimum was obtained with the N52 magnets orientated perpendicular to the 2D MOT laser beams, located with their closest face coincident with a plane 65.1 mm from the center of the chamber, their base offset by 20.5 mm from the laser beams, with dimensions $11 \times 38 \times 7 \text{ mm}^3$, and with their largest faces orientated toward the atoms as shown in Fig. 10. This produces a field gradient of 3.7 mT cm^{-1} on each axis in the xy plane at the center of the chamber, and the calculated field at all locations was used in the AtomECS atom-capture simulation.

Rotating the magnets such that they faced toward the atoms would have resulted in a greater field gradient per unit magnet volume, with the optimum angle calculated as around 20° . However, use of this angle would only have reduced the magnet volume by 10% with a similar reduction in the stray field gradients introduced in Chamber 2. Given the increased design complexity of machining angled magnet holders, it was decided to adopt perpendicular permanent magnets.

The simulated rate of atom loading was found to be approximately equal for magnet-to-atom distances varying by $\pm 5 \text{ mm}$. Our design also includes paired solenoid coils that allow for trimming of the field gradient for later empirical optimization and also for the application of bias magnetic fields in order to control the location of the 2D MOT—an important parameter since the atoms are then launched through a 3 mm diameter differential aperture between the two chambers.

The trimming coils consist of four water-cooled aluminum tape coils made of 30 mm wide and 0.2 mm thick anodized aluminum tape, supplied commercially as a custom design by Anoxal.¹¹ The use of aluminum tape resulted in compact, robust coils that self-insulate through anodization of the aluminum layers, despite supporting current densities of up to 10 A mm^{-2} . Aluminum has a lower electrical conductivity than copper, but the constrained space meant that overall volume drove our design requirements. The high thermal conductivity of aluminum combined with no need for electrical insulation between coil

layers permitted cooling from a single contact point, away from the atoms, via a copper heat-exchanger (visible in Fig. 10) coupled via a $3 \text{ W m}^{-1} \text{ K}^{-1}$ silicon pad.

After the iterative field and atom dynamics simulations had been performed, a final simulation was made using a commercial FEM software package, to confirm agreement with the simplified model of the permanent magnet fields and to characterize the additional effect of the trimming coils. Good agreement between the models was found. The trim coils should supply up to an additional 2.4 mT cm^{-1} if operated at their maximum capacity, allowing for a large range of adjustment from the baseline provided by the permanent magnets.

In addition, axial compensation fields are applied through similar, tape-wound coils (24 mm) from the same supplier. Since they provide only bias field compensation requiring currents $< 5 \text{ A}$, passive cooling sufficed.

By minimizing the volume requirements of chamber 1 coils, it was possible to place permanent magnets housed in aluminum casings close to the atoms, reducing their required volume and, therefore, minimizing the effect of stray fields in chambers 2 and 3. The magnet arrangement around chamber 1 and the resultant magnetic field profile are shown in Fig. 10. The field measured along one axis from two magnet pairs is shown in Fig. 11: the dashed and dashed-dotted lines are linear fits to the data over a range of positions including that required for operation. The difference between the fits illustrates the effect of applying a current to a trimming coil.

3. Magnet design—Chamber 2

In chamber 2, all fields are produced through electromagnets, making it possible to control the gradient over a large range and to ramp the total field to zero. The two chamber 2 magnet assemblies each contain two coils of square-profile, $5 \times 5 \text{ mm}^2$ hollow copper conductor with 3 mm internal apertures, cooled by internal water flow. These were wound in two parts as 5×4 - and 4×4 -turn coils embedded into the same housing—see Fig. 12. The conductor was first

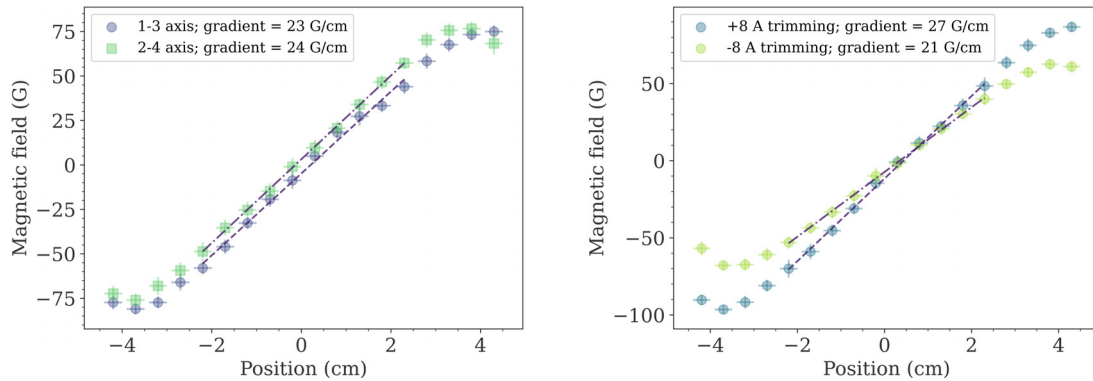


Fig. 11. (Left) Magnetic field in chamber 1 generated along two perpendicular axes by two pairs of permanent magnets, arranged in the design configuration. The magnetic field gradient in the center of the chamber is slightly less than the 27 G/cm predicted by simulations and has been found to vary by up to 2 G/cm depending on the individual installation. (Right) Magnetic field in chamber 1 generated along the “1–3” axis by the design configuration of two pairs of permanent magnets and trimming coils, with a trimming current of 8 A applied to all coils. Coils can be tuned independently to modify the field gradient and zero-field location. Data were measured by the University of Cambridge team.

insulated with heat-shrink PVC tubing before being wet-wound with Stycast resin.

The coils are electrically connected in series and the assemblies are run in anti-Helmholtz configuration. Cooling water is run in parallel through the four coils to reduce pressure requirements. An auxiliary, passively cooled winding was placed around the outer diameter of the coil closest to the atoms to provide DC offset field trimming, and thermocouples were embedded for interlocking and monitoring.

Figure 13 shows the axial magnetic field in chamber 2 generated by the magnet assemblies in the design configuration. The field gradient of 0.39 G/cm/A in the trap center is in good general agreement with field simulations assuming an insulating layer 0.6 mm thick surrounding each wire. Deviations from this simulation can be explained by inhomogeneities in the coil winding and casting and tolerances in the installation configuration. With water cooling, currents of up to 200 A have been continuously applied without the coils exceeding a temperature of 30 °C.

The self-inductance of the pair of coils installed in series and in anti-Helmholtz configuration around the chamber is <math><400 \mu\text{H}</math>,

allowing the current to be ramped within 1 ms from around 130 to 10 A, as required for the transition from blue MOT to red MOT, at a reverse voltage of 40 V.

IV. LASER-STABILIZATION SYSTEM

A. Motivation

The laser requirements were briefly outlined in Sec. II, and a level scheme including all the required laser wavelengths is shown in Fig. 1. The lasers at 461 nm (blue MOT), 679 and 707 nm (repumping) only require stabilization at the 1 MHz level. This stabilization was implemented using a software-based PID lock to a commercial wavelength meter, the High Finesse WS8.

Two of the lasers—those at 689 nm (red MOT) and 698 nm (atom interferometry)—have stringent frequency stabilization requirements that are the focus of this section. In order to create consistent atom samples in the narrowband stirred red MOT¹² and in order to match consistently the MOT position to the location of the dipole trap,⁷ the 689 nm laser must be stabilized at roughly the 2 kHz level or better. The 698 nm laser must be stabilized at roughly the 10 Hz level,

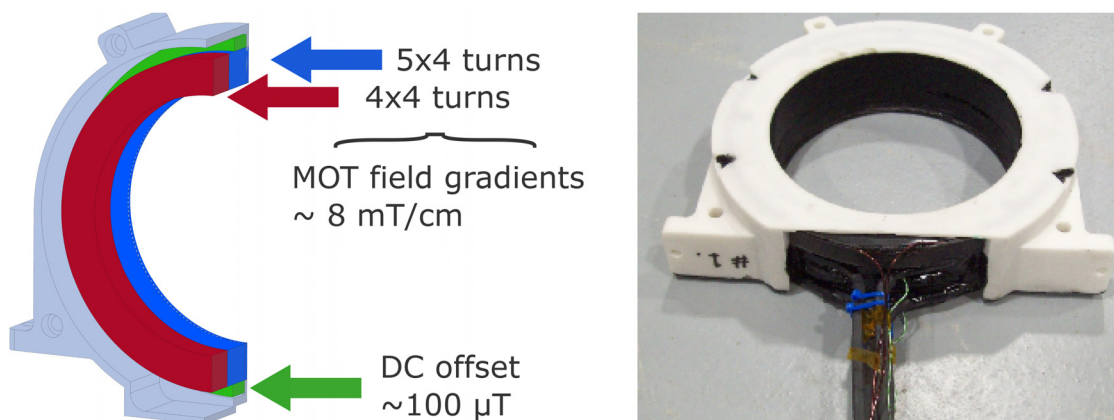


Fig. 12. (Left) Chamber 2 copper coil body showing the three individual coils involved. The red and blue coils are water-cooled in parallel but electrically connected in series and are capable of supporting 200 A of current flow indefinitely. (Right) A completed chamber 2 coil assembly, showing the 3D-printed resin former and Stycast potting. The semi-rigid current leads were intentionally left long so that water connections could be made far from sensitive optics to lower the risk of water damage.

10 April 2024 08:30:19

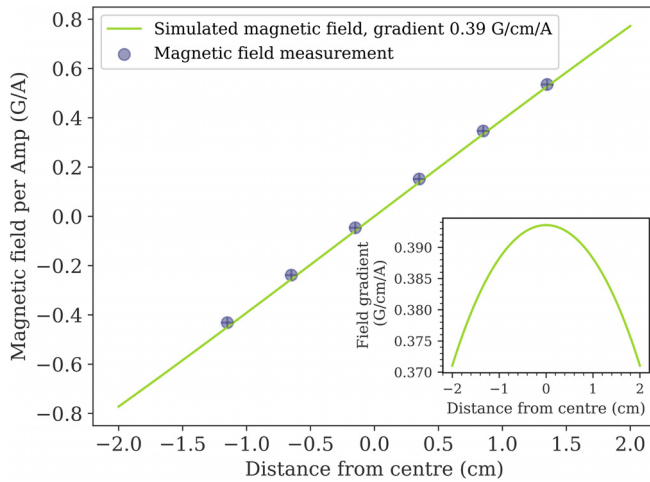


FIG. 13. The axial magnetic field in chamber 2 generated by two pairs of electromagnets, arranged in the design configuration. (Measured at a current of 10 A.) The measured data points indicate a gradient in agreement with that of a simulated field created by electromagnets in the design configuration with a layer of insulation 0.6 mm thick surrounding each wire. The inset shows the simulated magnetic field gradient in the center of the coil array. Data were measured by the University of Cambridge team.

in order to support high-fidelity π -pulses on the clock transition as needed for large momentum transfers.^{13,14}

B. Design

Informed by these requirements, a system to frequency-stabilise both the 689 and 698 nm light was designed. The fundamental aspects of the system are shown in Fig. 14. The 689 and 698 nm beams propagate in opposing directions through a notched cavity,¹⁵ purchased from stable laser systems.¹⁶ The transmitted and reflected wavelengths from each laser are then separated onto different photodetectors.

1. Description of cavity system, including optics

The optical layout used for laser stabilization is depicted in Fig. 14. A fraction of the light is split off from each of the main lasers at 689 and 698 nm and passed through a fiber-pigtailed waveguide

EOM (Jenoptik PM705). This light then exits the fiber and is collimated by an aspheric lens. An optical isolator is used to avoid the reflection of light back to the main laser and to suppress parasitic etalons between the cavity and the optical fiber tips. Following this, the light passes through a polarizing beamsplitter cube (PBS) and a quarter-wave plate. Any non-resonant light that is reflected from the cavity then passes through the same quarter-wave plate again, and the light exits the PBS using the other, orthogonal, port. Diffraction gratings are used to separate spatially the reflected beams at one wavelength from the transmitted beam at the other wavelength—a dichroic beamsplitter would be mechanically more convenient, but an appropriate optic was difficult to source because the laser wavelengths are close to each other. The transmitted beam provides a discriminator signal that helps relock the laser frequency following any disturbances.

2. Pound-Drever-Hall method and reference

To generate an error signal with which the laser frequency is stabilized, the Pound-Drever-Hall (PDH) method is used.¹⁸ This technique is widely employed in precision measurement, spectroscopy, and optical communications. It involves feeding back a portion of the laser light that has been reflected from the reference cavity to the laser’s frequency control system. In the AION system, a fiber-based electro-optic modulator (EOM) is used to modulate the laser light at around 10 MHz. Upon interaction with the cavity, this light is then converted to an electrical signal on a fast photodiode (Koheron PDX10S-5-DC-SI), which is then mixed with a local oscillator, generating an error signal proportional to the frequency difference between the laser and the cavity. The error signal is fed back to the laser frequency control system, which adjusts the laser frequency to reduce the error signal.

In order to lock the laser at a frequency corresponding to the atomic transition, which can be as much as half of the free spectral range ($\omega_{FSR}/2 = 2\pi \times 750$ MHz, away from the nearest (randomly positioned) cavity mode, a dual sideband lock is applied.¹⁷ In this method, sidebands are created by driving the EOM with an offset frequency ω_{offset} that is much larger than the PDH modulation frequency ω_{PDH} . The laser is tuned and locked such that the frequency of the first-order sideband at $\omega_{laser} \pm \omega_{offset}$ is resonant with the cavity. With the offset frequency’s amplitude chosen appropriately to suppress the carrier component of the laser field, this method results in two possible lock-points within each ω_{FSR} frequency range of the cavity, separated by ω_{offset} ; only one of which is desirable. Since ω_{offset} is

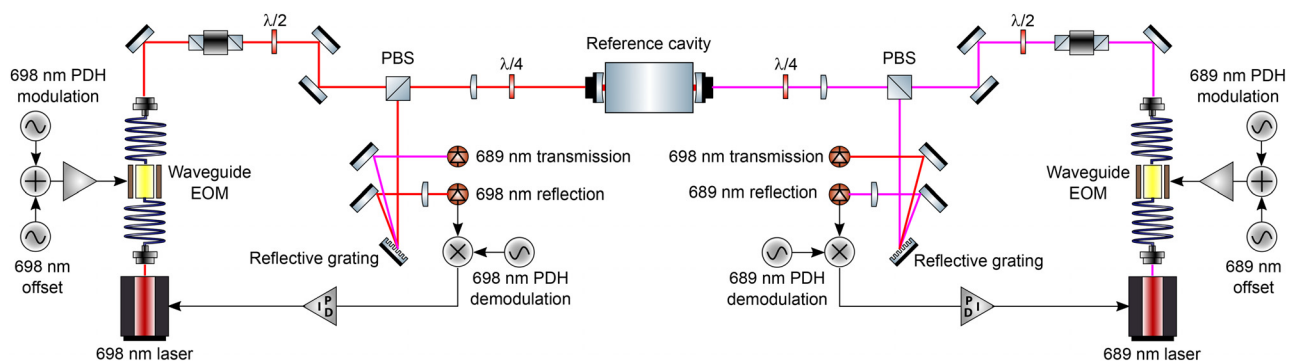


FIG. 14. Optical layout for locking the 689 and 698 nm lasers to an optical reference cavity, using a dual-sideband PDH lock.¹⁷

10 April 2024 08:30:19

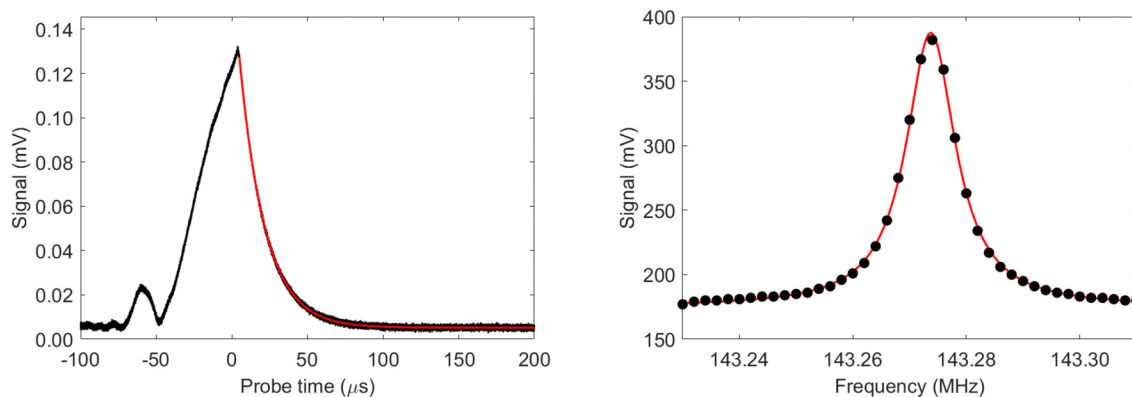


FIG. 15. (Left) Cavity ringdown measurement at 689 nm. The data are fitted with an exponential decay, giving a lifetime of 16.9 μs , implying a finesse of 160 000. (Right) Cavity linewidth. The cavity linewidth is determined using a photodiode to measure light transmitted through the cavity as the laser frequency is scanned across the resonance. Fitting the transmission data gives a FWHM of 10.6 kHz. Data were measured by the Rutherford-Appleton Laboratory team.

typically several hundred megaHertz, a commercial wavemeter is able to disambiguate the modes when the laser requires initial locking.

3. Parallel construction and characterization

Due to their centralized construction, the cavities could be compared with each other, to diagnose characteristics, such as cavity mode linewidth, locked-laser linewidth, and short-term frequency instability. These comparisons could be done by locking separate lasers to their own cavity and performing a heterodyne measurement between the lasers. However, an alternative method is to use just one laser, combined with the dual sideband generation technique. The first cavity is used to lock the laser frequency directly to the cavity mode without offset, as described in Sec. IV B 2. Then, a fraction of this light is brought into resonance with a second cavity. This is done by adding a second frequency to the EOM, which supplements the modulation used to derive the PDH signal. As the free spectral range of the cavity is 1.5 GHz, this again means that the additional frequency may need to be anything up to 750 MHz in order to bridge the gap. To account for the cavity mode drift, this additional frequency needs to be tracked and counted. In the AION implementation, the relatively slow drift of the cavities means that a low-bandwidth PID lock—which feeds back onto the EOM frequency—is sufficient.

This comparison setup underpins the data presented in Fig. 15, which show that the cavities have sufficient finesse to lock the lasers at the Hertz level. Further measurements with an RF spectrum analyzer and a frequency counter verified that the laser sidebands could be locked to separate cavities to a relative linewidth of 10 Hz, with a frequency instability of 3 Hz at 1 s averaging time.

4. Conclusion and benefits of parallel construction of the laser stabilization systems

The laser stabilization systems for all five strontium laboratories were built in parallel in one location, at RAL, before being distributed to the partner institutions, as shown in Fig. 16. The approach of parallel construction had several advantages for the project.

The primary motivation, and subsequent benefit, of this approach was efficiency. By centralizing the design and construction, an

optimized, more streamlined process was developed, harnessing the expertise of team members with prior experience working with ultra-stable laser systems. By doing so, the systems could be constructed more efficiently and in a shorter time frame than had they been assembled locally at each institute.

With the laser stabilization systems co-located, it was possible to characterize them against each other; a key advantage not afforded by local assembly. It is anticipated that in the future more efficient debugging, maintenance, and operation of the laser stabilization systems will be possible in the five collaborating laboratories, with rapid and transparent sharing of experience between them.

V. COLD ATOM COMMISSIONING

A. Strontium oven

The sidearm design has been validated by demonstrating first-stage cooling of strontium in a 2D MOT in chamber 1 and a first 3D blue MOT in chamber 2. As a first step, the atomic beam coming out of the oven was observed through fluorescence and absorption spectroscopy on the broad blue transition, as seen in Fig. 17 for various oven temperatures.

For the first MOTs, the strontium oven was heated to 420 °C, which raised the pressure in chamber 1 from 5.7×10^{-10} mbar at 22 °C to 6.5×10^{-9} mbar, as deduced from the ion-pump current. This oven temperature is low compared to the sublimation temperature of strontium and will be increased as the atomic flux of the sidearm is optimized. The oven design has been tested at temperatures of up to 650 °C.

B. 2D blue MOT

In order to trap atoms in the 2D blue MOT, light detuned by -2Γ from the 1S_0 to 1P_1 transition in ^{88}Sr is used. Initial testing employed ^{88}Sr , due to its natural abundance and bosonic nature, easing some of the frequency requirements of the laser system. Two circularly polarized 45 mm beams of intensity 23.0(5) and 26.0(5) mW cm^{-2} were delivered into the 2D MOT chamber and retro-reflected to create the four trapping beams. A 2D MOT of order 20 mm in the untrapped dimension was observed in chamber 1 (see left panel of Fig. 18). An atomic beam was created with the

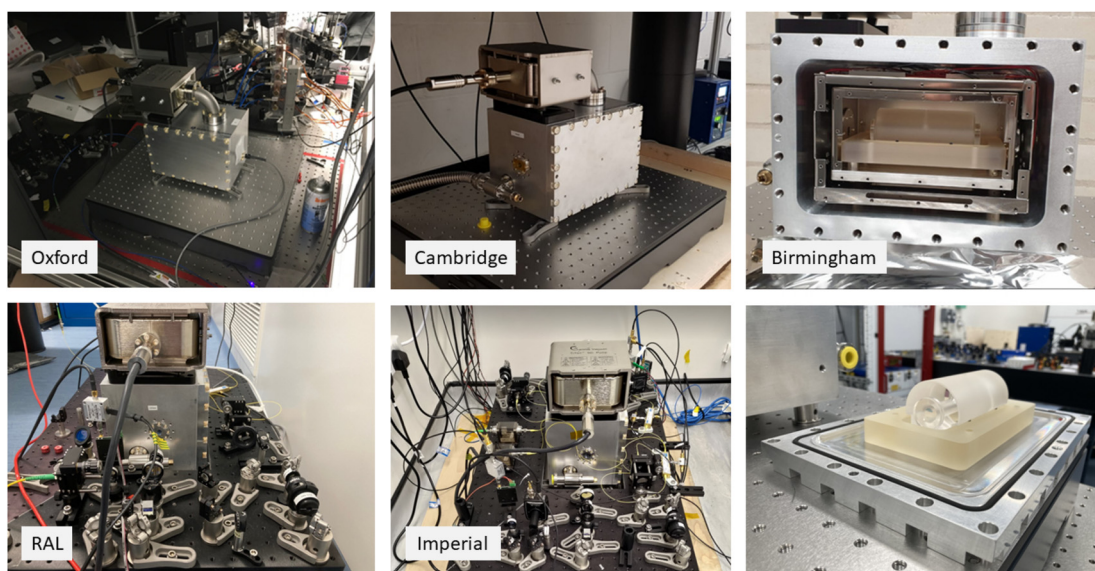


Fig. 16. Cavity assemblies. The five cavity systems at various stages of construction. Also shown (lower right) is a cavity prior to installation inside the vacuum housing. All optics were assembled centrally prior to delivery. Cavities were transported outside of their vacuum housing and reassembled locally at each institute.

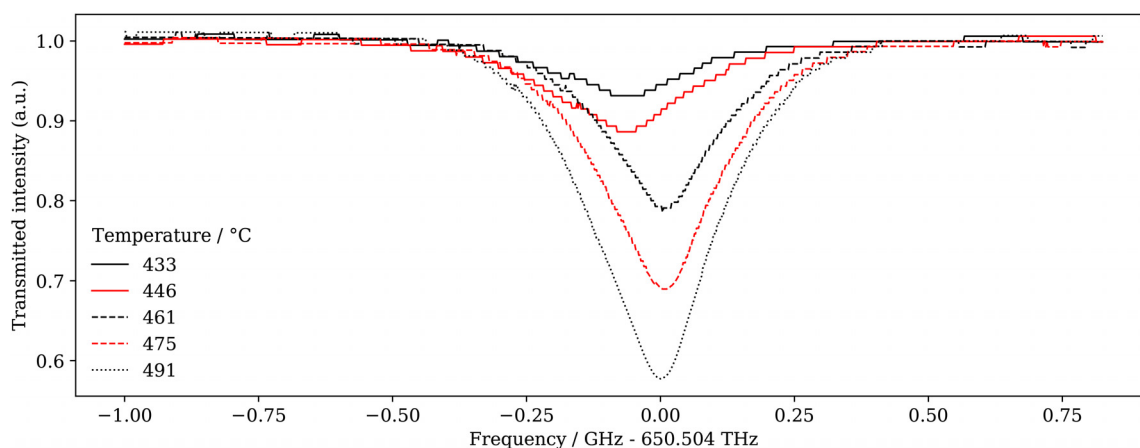


Fig. 17. Absorption spectra of the atomic beam at various oven temperatures. The laser beam was normal to the atomic beam and the transverse velocity distribution is non-Gaussian for atoms effusing through the cylindrical channels in the nozzle (see Fig. 3) of the oven.¹⁹ Data were measured by the Cambridge team.

addition of a near-resonant weak push beam along the un-trapped axis to guide atoms from chamber 1 to chamber 2, via the 3 mm differential pumping aperture. In this test, the magnetic fields for the 2D blue MOT were supplied from the permanent magnets only, but they can be tuned in the future using the coils to optimize the atom flux through the system.

C. 3D blue MOT

An initial 3D MOT was loaded in chamber 2 from the pre-cooled atomic beam from the 2D MOT (see right panel of Fig. 18). For the 3D blue MOT, three circularly polarized orthogonal beams of 15 mm at 32, 36, and 18 mW cm⁻², were retro-reflected to create the six

trapping beams, and detuned by -2Γ from the 1S_0 to 1P_1 transition in ^{88}Sr . A higher laser intensity is used along the radial 3D MOT axes, as opposed to the MOT coil axis, to improve the capture velocity for atoms entering from the radial direction. 679 and 707 nm lasers (Fig. 1), resonant with their respective transitions, were used to pump back into the cooling cycle atoms that fall into the 3P_0 and 3P_2 states. A current of 125 A was used in the quadrupole coils to provide a field gradient of 4.9 mT cm⁻¹.

D. Atom flux measurement

The performance of the 2D blue MOT can be assessed from the loading rate, τ , and the equilibrium atom number, N_{eq} , of the 3D blue

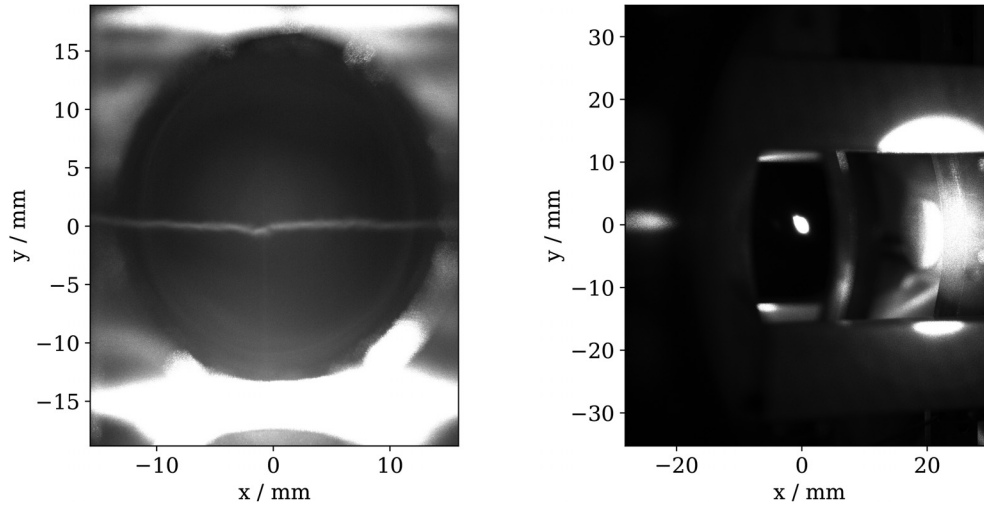


FIG. 18. (Left) Fluorescence from strontium atoms in the 2D blue MOT in the Imperial sidearm’s chamber 1, viewed orthogonally to the push beam axis. Atoms are laser-cooled and compressed radially with minimal confinement along the longitudinal, push-beam axis, resulting in an elongated cloud visible as the thin, gray line stretching horizontally across the frame. (Right) Image of a 3D blue MOT in chamber 2, captured from the atoms pushed by the 2D MOT in chamber 1. The strontium cloud is visible as a small spot in the center of the frame, and the surrounding structure is an optical cavity spacer used for creating squeezed quantum states that is unique to the Imperial sidearm variant. All spatial dimensions are given in the focal plane of the atom clouds. Images were taken by the Imperial team.

MOT in chamber 2. The number of atoms, N , at a time, t , of the MOT is given by²⁰

$$N(t) = N_{eq}(1 - \exp(-t/\tau)). \quad (5.1)$$

Our preliminary results can be seen in Fig. 19, where the loading rate of the 3D MOT is shown for two atomic beam cases: with the 2D MOT and push beam on and with just the 2D MOT light on in chamber 1. In each case, the oven temperature was kept constant, all intravacuum valves remained open, and the 3D MOT light kept on. The 3D MOT coils were turned on at $t = 0$ s to load the 3D MOT in each

case. 10^8 atoms were loaded into the 3D MOT trap, with a loading time constant of 198.8(2) ms estimated from the fit. The loading rate and atom number can be increased further by increasing the oven temperature to optimize the atom flux. In the cases where the push beam was shuttered, the loading rate of the 3D blue MOT dropped to zero. This shows that leakage from the 2D MOT, and diffusion from chamber 1 to chamber 2 through the differential pumping aperture, is negligible. Loading from background vapor in chamber 2 is also not seen, suggesting that the partial pressure of strontium in chamber 2 is low.

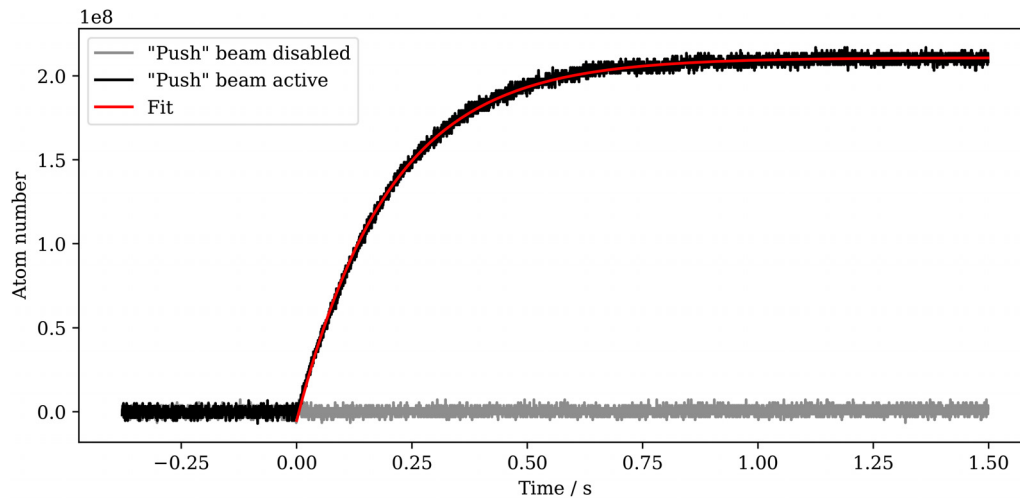


FIG. 19. The 3D MOT loading curve from the 2D MOT atomic beam. MOTs of order 10^8 atoms are loaded with time constant of 198.8(2) ms, as measured by an exponential fit as in Eq. (5.1) that is represented by the red line. With the push beam off, there is no loading seen from the 2D MOT alone, showing no diffusion through the 3 mm differential pumping aperture. Data were measured in the University of Birmingham sidearm.

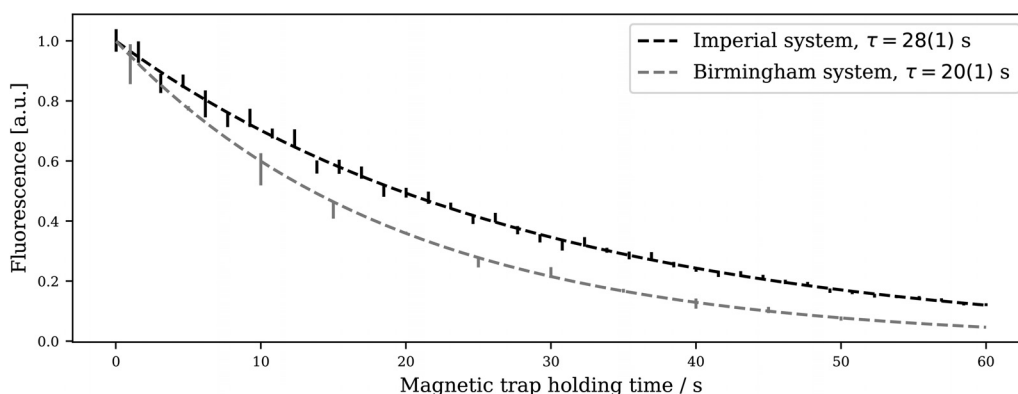


FIG. 20. The lifetimes of the magnetic traps for atoms in the $^3P_{2m_F=2}$ state in the Imperial and Birmingham sidearms. The figure shows the level of background-corrected fluorescence measured from atoms recaptured in the 1S_0 to 1P_1 MOT after holding atoms for a variable length of time in the magnetic trap. Fitted time constants of 28(1) and 20(1) s were measured from ten and four repeats of each holding time for the Imperial College and University of Birmingham sidearms, respectively. Standard errors from these repeats are shown. These lifetimes exceed the length of experiments that will take place in these chambers, demonstrating suitable vacuum quality and providing a measure of the pressure at the atoms' location of order 1×10^{-10} mbar.

In order to assess the vacuum performance independently from the ion pump values, the loss rate of atoms from a magnetic trap²¹ was used to estimate the dominant collision rates within the system, and thus, the pressure of the system. Atoms are loaded into a MOT for 4–5 s and pumped into the magnetically trappable substates of the 3P_2 state by turning off the repump lasers. The atomic beam and 3D MOT light is shut off and the atoms are held in the 3D magnetic trap for a variable hold time, before the repump lasers and 3D MOT light is flashed on. Fluorescence from the remaining atoms is measured with a photodiode and imaging telescope. Figure 20 shows the magnetic trap lifetime, where the population decays with a time constant of 28(3) and 20(1) s for the Imperial and Birmingham sidearms, respectively. Using the calibration given in Ref. 21, the pressure in chamber 2 is estimated to be $1.0(1) \times 10^{-10}$ and $1.7(1) \times 10^{-10}$ mbar, respectively. The lifetime of the atoms in the magnetic trap far exceeds the length of an experiment in these systems.

VI. DISCUSSION

The successful delivery of the five UHV systems to the individual institutes in a timely fashion was facilitated by the centralization of three core activities that were outlined above:

- Design;
- Manufacture and assembly;
- Delivery and logistics.

The engineering design process started in April 2020 and ran through to December 2021. During this period, the design was taken from a first concept to a fully detailed and analyzed design ready for manufacture and commissioning. This centralized design process was led by an engineer at the University of Oxford. While not necessarily being faster than a traditional design process for an individual setup, crucially the centrally coordinated structure provided for the required compatibility of the resulting systems that will allow AION to port technologies and cold atom advances between institutions and to the main instruments. It, furthermore, allowed for several benefits that

increased the efficiency of the design engineering process that included:

- Resource optimization—A centrally coordinated engineering effort means that the use of engineering resource can be optimized, leading to a reduction in duplication of effort and the ability to ensure that the right people are working on the appropriate tasks, improving productivity, and reducing costs;
- Standardization—this increases the speed of the design process, due to a reduction in errors, and the ability to learn from and carry fixes and improvements across systems;
- Communication—communications between team members with engineering responsibilities can be improved, reducing and minimizing miscommunications. This, in turn, allows a more agile work model and faster decision-making;
- Expertise—a common resource pool of engineering talent means that a wider skill set will be available across the project. This is particularly useful for issues that require specialized skills to resolve, such as UHV design, pumping calculations, and optomechanics—all of which were present in this phase of the project;
- Risk mitigation—a central point of contact can ensure that better and more consistent controls and mitigation techniques are used to improve risk mitigation. This, in turn, reduces failures and improves the efficiency of the engineering process.

All of the above-mentioned benefits were realized for the project and improved both the quality of the engineering design work and the rate at which it was completed, though it is difficult to quantify the time saved during the design phase by the centralized process.

It is much easier to quantify the efficiency gains for the manufacturing and assembly process. During this phase of the project, the rate at which a UHV system could be built and commissioned was accelerated greatly. This was primarily due to carrying the knowledge gained by building one system over into the subsequent builds. The continuity and accumulation of knowledge would be lost in a non-centralized process. A second, strongly linked benefit was the creation and development of a facility with a dedicated skillset focused on the

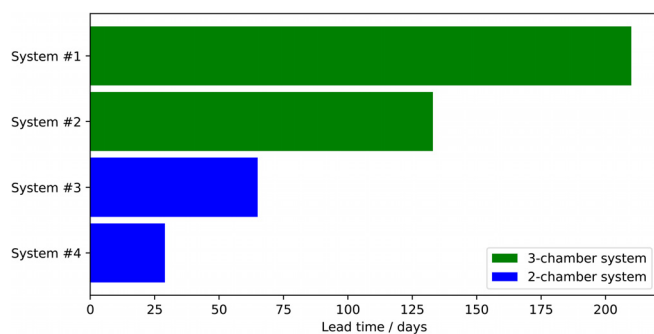


Fig. 21. Evolution of the build times (in days) of the four centrally produced UHV systems (3-chamber systems in green and 2-chamber systems in blue) as the project progressed. The build time for the Imperial College UHV system is not shown: it was not built centrally since it required specific in-vacuum hardware for quantum squeezing measurements and a specialized build process.

requirements of this specific UHV-system build. Figure 21 shows the build-time duration in days for each system that was built via the centralized process. The four centralized builds are shown and split into 3-chamber and 2-chamber systems. The decrease in build-time from system to system can be seen clearly. A more detailed list of reasons why the centralized approach increased the efficiencies of the system builds is as follows:

- Continuity of knowledge—the lessons learnt, knowledge, and skills gained from the prior builds directly benefited the subsequent builds;
- Inventory management—a centrally managed inventory of long-lead-time parts (such as coated viewports) enabled the utilization of stock items of later builds in the prior builds when there were failures and difficulties during bake cycles. The used stock could then be re-ordered in advance, minimizing delays on the subsequent systems;
- Parallel builds—agile planning and workflow were facilitated by the centralized, coordinated approach, which enabled parallel system builds to be carried out. As one system would undergo its bakeout, a second system could be built and assembled. This yielded large efficiency gains;

All of the above-mentioned contributed to the build-speed increases shown in Fig. 21 and made for very significant gains. The entire engineering process, during which all five UHV systems went from conceptual design to fully delivered systems, took approximately two years and seven months. Within this period, engineering design took approximately one year and eight months, with manufacture and delivery taking just under a year.

VII. SUMMARY AND CONCLUSION

Equipping five ultra-cold strontium laboratories (UCSLs) was motivated by the AION plan to grow dedicated cold atom expertise in strontium around the UK and to enable parallel R&D efforts toward the required design objectives for the atom sources for later stages of the AION project, including the transport and launch of atoms, large momentum transfers, squeezing and high-sensitivity atom interferometry. This plan presented the collaboration with the challenge of

building five compatible state-of-the-art UCSLs in parallel, which has had no precedent in the field of cold atom physics.

This document has described the approach taken by the AION collaboration, namely, the centralized design and production of key components of the UCSLs. This approach was familiar to high-energy physicists but was a novelty for the cold atom community, where typically every setup has bespoke requirements. It enabled the construction of multiple UCSLs faster and more cost-effectively than following the “in-house” approach that has typically been taken by the latter community. This document focused on the ultra-high-vacuum (UHV), magnet, and laser-stabilization (LS) systems, but similar coordinated approaches are also being followed regarding control software and optical design. Commissioning data on the performances of the UHV, magnet, and LS systems obtained by AION UCSL teams have also been presented.

The centralized approach ensured maximal commonality between the equipment in five state-of-the-art UCSLs across the UK. Following their construction, the required R&D into improved cold-strontium quantum technology can be performed over the next decade. This approach provided economies of scale in the design and production process and is expected to provide benefits also in the operations of the UCSLs.

The shared approach between the particle and cold atom groups in the different participating universities and national laboratories has helped foster a national community combining the expertises of members of the previously disjoint EPSRC and STFC communities, which may provide the basis for future valuable cross-fertilization.

The AION experience could serve as a useful model for the modular and distributed development and construction of other cold atom projects, such as atomic clock experiments or neutral atom quantum computing systems. This model could become increasingly useful as the range of industrial applications of cold atom systems broadens in the coming years. International opportunities are already being explored. For these reasons, the AION collaboration is investigating the possibility of commercializing its approach and establishing dedicated design and/or production units at National Laboratories, such as RAL and Daresbury.

ACKNOWLEDGMENTS

This work was supported by UKRI through its Quantum Technology for Fundamental Physics programme, via the following grants from EPSRC and STFC in the framework of the AION Consortium: ST/T006536/1 and ST/W006448/1 to the University of Birmingham; ST/T006579/1, ST/W006200/1, and ST/X004864/1 to the University of Cambridge; ST/T007001/1 to the University of Liverpool; ST/T006994/1 and ST/W006332/1 to Imperial College London; ST/T00679X/1 to King’s College London; ST/T006633/1 to the University of Oxford; and ST/T006358/1 and ST/W006510/1 to the STFC Rutherford-Appleton Laboratory. L.B. acknowledges the support from the STFC Grant No. ST/T506199/1. D.B. was supported by a “Ayuda Beatriz Galindo Senior” Grant from the Spanish Ministerio de Universidades (No. BG20/00228). I.F.A.E. was partially funded by the CERCA program of the Generalitat de Catalunya. J.M. acknowledges the support from the University of Cambridge Isaac Newton Trust. J.S. acknowledges the support from the Rhodes Trust. The Cambridge team thanks X. Su and M. Zeuner for support in earlier stages of this project. The Rutherford Appleton Laboratory team thanks S. Canfer, B. Green, S. Greenwood, P. Jeffery, D. Tallentire, and

J. Tarrant for their valuable input and contributions to the design process of the assemblies and during the building of the sidearms. For the purpose of open access, the authors have applied for a Creative Commons Attribution (CC-BY) license to any Author Accepted Manuscript version arising from this submission.

AUTHOR DECLARATIONS

Conflict of Interest

The authors have no conflicts to disclose.

Author Contributions

All authors have contributed equally to this paper.

Oliver Buchmueller: Writing – review & editing (equal).

DATA AVAILABILITY

The data that support the findings of this study are available from the corresponding author upon reasonable request.

REFERENCES

- ¹L. Badurina *et al.*, *J. Cosmol. Astropart. Phys.* **5**, 011 (2020).
- ²AION collaboration, O. Buchmueller *et al.*, see <https://aion-project.web.cern.ch/> for “The Atom Interferometric Observatory and Network: exploration of ultra-light dark matter and gravitational waves.”
- ³L. Badurina, O. Buchmueller, J. Ellis, M. Lewicki, C. McCabe, and V. Vaskonen, *Philos. Trans. R. Soc. A* **380**, 20210060 (2021).
- ⁴J. E. Greene, J. Strader, and L. C. Ho, *Annu. Rev. Astron. Astrophys.* **58**, 257 (2020).
- ⁵AEDGE collaboration, Y. A. El-Neaj, *et al.*, *EPJ Quant. Technol.* **7**, 6 (2020).
- ⁶UKRI, see <https://uknqt.ukri.org/our-programme/qitfp/> for “UK National Quantum Technologies Programme—Quantum Technologies for Fundamental Physics.”
- ⁷S. Stellmer, R. Grimm, and F. Schreck, *Phys. Rev. A* **87**, 013611 (2013).
- ⁸B. J. DeSalvo, M. Yan, P. G. Mickelson, Y. N. Martinez de Escobar, and T. C. Killian, *Phys. Rev. Lett.* **105**, 030402 (2010).
- ⁹X. Chen, M. Zeuner, U. Schneider, C. Foot, T. Harte, and E. Bentine, “Atomecs: Simulate laser cooling and magneto-optical traps,” [arXiv:2105.06447](https://arxiv.org/abs/2105.06447) (2021).
- ¹⁰M. Ortner and L. G. Coliada Bandeira, *SoftwareX* **11**, 100466 (2020).
- ¹¹“Anoxal GmbH.” <https://www.anoxal.com/>.
- ¹²T. Mukaiyama, H. Katori, T. Ido, Y. Li, and M. Kuwata-Gonokami, *Phys. Rev. Lett.* **90**, 113002 (2003).
- ¹³S.-w. Chiow, T. Kovachy, H.-C. Chien, and M. A. Kasevich, *Phys. Rev. Lett.* **107**, 130403 (2011).
- ¹⁴J. Rudolph, T. Wilkason, M. Nantel, H. Swan, C. M. Holland, Y. Jiang *et al.*, *Phys. Rev. Lett.* **124**, 083604 (2020).
- ¹⁵S. Webster, M. Oxborrow, and P. Gill, *Phys. Rev. A* **75**, 011801(R) (2007).
- ¹⁶“Stable Laser Systems.” <https://stablelasers.com>.
- ¹⁷J. I. Thorpe, K. Numata, and J. Livas, *Opt. Express* **16**, 15980 (2008).
- ¹⁸R. W. P. Drever, J. L. Hall, F. V. Kowalski, J. Hough, G. M. Ford, A. J. Munley *et al.*, *Appl. Phys. B* **31**, 97 (1983).
- ¹⁹P. T. Greenland, M. A. Lauder, and D. J. H. Wort, *J. Phys. D* **18**, 1223 (1985).
- ²⁰R. W. Moore, L. A. Lee, E. A. Findlay, L. Torralbo-Campo, G. D. Bruce, and D. Cassettari, *Rev. Sci. Instrum.* **86**, 093108 (2015).
- ²¹S. B. Nagel, C. E. Simien, S. Laha, P. Gupta, V. S. Ashoka, and T. C. Killian, *Phys. Rev. A* **67**, 011401(R) (2003).